Thermal stability of ultrasoft Fe–Zr–N films

2003 J. Phys.: Condens. Matter 15 7663

(http://iopscience.iop.org/0953-8984/15/45/005)

INSTITUTE OF PHYSICS PUBLISHING JOURNAL OF PHYSICS: CONDENSED MATTER

J. Phys.: Condens. Matter **15** (2003) 7663–7674 PII: S0953-8984(03)64337-7

Thermal stability of ultrasoft Fe–Zr–N films

N G Chechenin[1,3], A van Veen[2], H Schut[2], A R Chezan[1], D O Boerma[4], T Vystavel[1] and J Th M De Hosson[1]

[1] Department of Applied Physics, Materials Science Centre and the Netherlands Institute for Metals Research, University of Groningen, Groningen, The Netherlands
[2] Interfaculty Reactor Institute, Delft University of Technology, Delft, The Netherlands
[3] Skobeltsyn Institute of Nuclear Physics, Moscow State University, 119899 Moscow, Russian Federation
[4] Centro de Micro-Analisis de Materials, Universidad Autonoma de Madrid, Cantoblanco, I-28049, Madrid, Spain

Received 2 June 2003
Published 31 October 2003
Online at stacks.iop.org/JPhysCM/15/7663

Abstract

The thermal stability of nanocrystalline ultrasoft magnetic $(Fe_{98}Zr_2)_{1-x}N_x$ films with $x = 0.10$–0.25 was studied using thermal desorption spectrometry, positron beam analysis and high resolution transmission electron microscopy. The results demonstrate that grain growth during the heat treatment is accompanied by an increase of the free volume and nitrogen relocation and desorption. All these phenomena can drastically degrade the ultrasoft magnetic properties. The nitrogen desorption has already started at temperatures around 400 K. Nevertheless, most of the nitrogen leaves the sample at a temperature above 800 K. We found that nitrogen out-diffusion is significantly retarded compared with the prediction of the diffusion in bulk α-Fe. A qualitative model is proposed in which the nitrogen out-diffusion in nanocrystalline material is retarded by trapping at immobile defects, namely Zr atoms, and also by voids at grain boundaries. From a certain temperature, nitrogen migrates from the interior of the nanograins to the nanovoids at the grain boundaries and the out-diffusion to the outer surface is controlled by transport between the voids.

(Some figures in this article are in colour only in the electronic version)

1. Introduction

Ultrasoft magnetic films with a low coercive magnetic field of ∼1–5 Oe, an induced uniaxial magnetic anisotropy of 10–50 Oe and a high saturation magnetization ∼15–20 kG are required for future high frequency applications in the gigahertz region. The grain size is a crucial parameter of the microstructure of a magnetic film: nanometre size of the grains is required for averaging out the magnetocrystalline anisotropy and for reduction of the intrinsic stray field [1, 2]. In films of the FeXN type, nitrogen serves as a grain refiner and the transition metal X = Ti, Cr, Zr, Ta etc as a nitrogen binder, favouring a high concentration of nitrogen

content [3]. Films of this type proved to give the required magnetic properties [4–7]. The introduction of soft magnetic materials into the integrated technology of high frequency inductors [8, 9] also placed a strong requirement on the thermal stability above 600 K. A similar constraint is imposed by the use of soft magnetic underlayers for the magnetic storage media with perpendicular magnetization and as material for writing heads [8].

The main emphasis of this study is on structural and compositional evolution during a thermal treatment in the temperature range up to 950 K and on the accompanying change of the magnetic properties of the Fe–Zr–N films. The microstructural evolution was investigated by means of x-ray diffraction (XRD), transmission electron microscopy (TEM) and high resolution transmission electron microscopy (HRTEM) (using an *in situ* heating stage), positron beam analysis (PBA) and thermal desorption spectrometry (TDS). TDS gives directly the amount of outgassed nitrogen during heat treatment. Positron annihilation was used as a probe for the free volume in the near-amorphous and recrystallized films. Due to the nanometre size of the grains, nearly all positrons diffuse to the grain boundaries and voids and then become trapped and annihilated. The size and character of the free volume on the atomic scale was monitored by PBA during thermal annealing, where two competing processes are involved: the reduction of the free space by the formation of dense grains and by a decrease of intergranular space during the grain growth on one hand and, on the other hand, an increase of the free volume due to nitrogen release. During this release gas-filled bubbles are formed, which we also consider as free space. We found out that the latter processes dominate, at least in the range up to 800 K. Preliminary results of this study have already been published elsewhere [10].

2. Experimental details

Fe–Zr–N films were prepared by DC magnetron reactive sputtering. Films with a thickness between 50 and 400 nm were deposited at several substrate temperatures between 220 and 480 K. The films were grown in a nanocrystalline structural state on glass or silicon substrates. Polymer or Cu underlayers were used to float the film on a grid for TEM investigation. The deposition conditions were chosen to obtain a desirable composition $(Fe_{98}Zr_2)_{1-x}N_x$ with x in the range up to 0.25. A uniaxial anisotropy was induced in the film, applying a magnetic field of 800 Oe in the plane of the samples during deposition. More details on the film deposition can be found in [7].

Several techniques were used to characterize the samples and their properties. Rutherford backscattering spectrometry (RBS) and elastic recoil detection (ERD) [11] were used to characterize the thickness and composition of the samples. A Philips PW1710 XRD spectrometer was used to characterize the texture and the size of the grains (using the Scherrer relation). The nitrogen content from the shift of the (110) bcc peak in XRD was also estimated, neglecting contributions of other factors such as elastic strains of the lattice. To study the microstructure, a transmission electron microscope JEOL 2010F was used, equipped with a heating stage double tilt goniometer and with a post-column energy filter.

Usually the films showed a texture with the $\langle 011 \rangle$ axis normal to the surface. The magnetic properties were found to depend on the grain size and nitrogen content. The nitrogen content was very high, between 10 and 25 at.%, as estimated from both ERD and the shift of the (011) bcc XRD line. The grain size, as determined from XRD, was in the range from 1.6 to 20 nm. This was in accordance with TEM and HRTEM observations; see e.g. figure 1. Films of this type had a very small coercive field, $H_c \approx 1$ Oe, a uniaxial anisotropy $H_k \approx 10$–25 Oe, a high magnetization value above 15 kG and a high frequency response in the gigahertz region [7, 12].

Positrons proved to be a sensitive probe for the free volume in the near-amorphous and recrystallized films [13]. PBA of the samples was performed with a variable energy positron

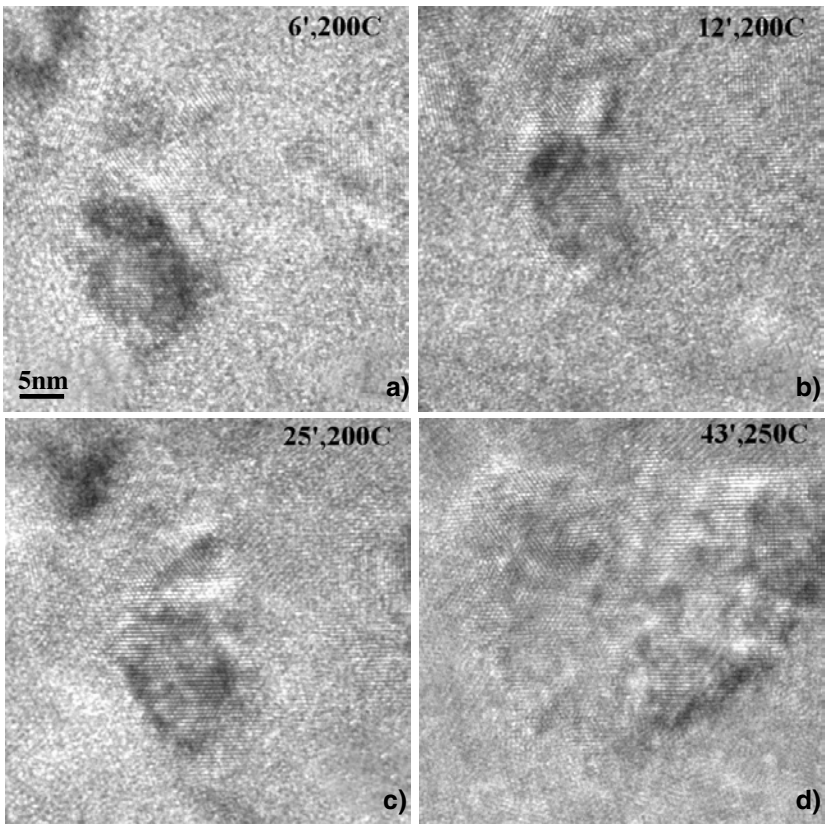

Figure 1. HRTEM observations of grain growth during *in situ* thermal treatment at: (a) 473 K, 6 min; (b) 473 K, 12 min; (c) 473 K, 25 min; (d) 523 K, 43 min.

(VEP) facility at IRI TU Delft. A positron beam obtained from a 40 mCi ^{22}Na source was used. After moderation of the energy in a 6 μm tungsten foil, the positrons were accelerated to energies between 1 and 30 keV and a current of 5×10^4 positrons s^{-1} was obtained. Annihilation γ-quanta, measured by a Ge detector, produce a peak centred at the energy of $E_\gamma = 511$ keV. The energy in each annihilation event is shifted due the Doppler effect by $\Delta E = pc/2$, where c is the light velocity and p is the momentum of the electrons, which depends on the site of annihilation. The shape of the peak is determined by the momentum distribution of the annihilated electrons because of Doppler broadening. In addition, the peak is broadened by the resolution of the detector.

TDS gives the amount of outgassed nitrogen during heat treatment. The sample was enclosed in a desorption volume (330 cm^3) of an UHV chamber (figure 2), with a base pressure of 1×10^{-7} Torr. The gas release during the processing was monitored in two ways. The experiment consisted of a series of heating–annealing–cooling–ageing cycles with 25 K temperature increase in each cycle. Using a membrane manometer, the total pressure increase in the desorption chamber was measured (figure 3). By sampling the gas in a small volume 1.72 cm^3, the mass spectra of the gas were measured, using a quadrupole mass spectrometer (QMS). Besides the nitrogen, there was a large fraction of hydrogen, carbon, atomic oxygen, oxycarbons and hydrocarbons in the QMS spectra of the released gas. Therefore, calibration was required to estimate quantitatively the amount of outgassed nitrogen. The molecular

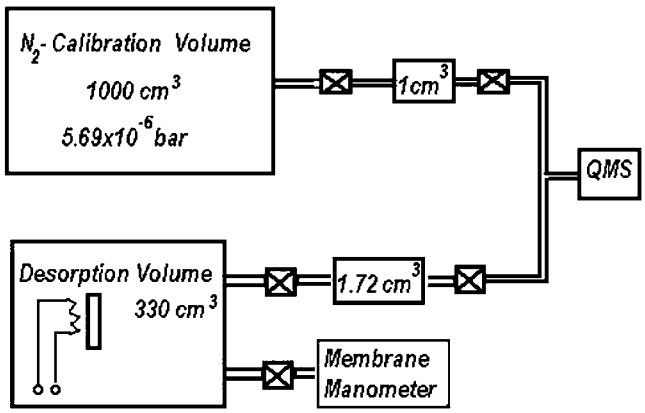

Figure 2. The experimental set-up for TDS.

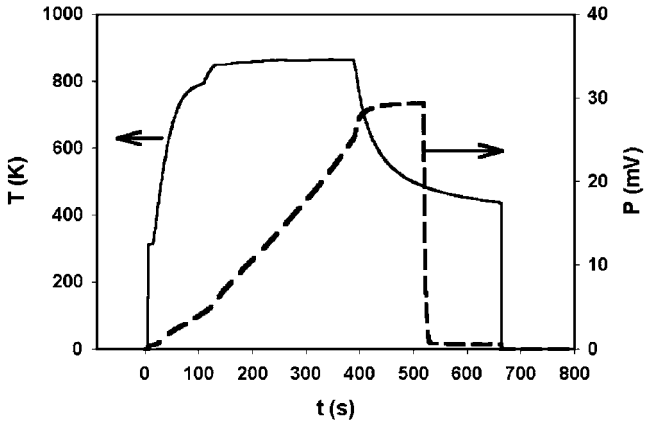

Figure 3. Temperature and pressure versus time for one of the cycles.

nitrogen ($M = 28$ au) lines interfered strongly with those from CO molecules whereas the atomic nitrogen line ($M = 14$ au) was easy to separate from the background even at a high temperature where the background strongly increased. For this reason, the atomic nitrogen line was used for the analysis.

For calibration, we used a standard 1000 cm^3 volume filled with pure nitrogen (99.995%) up to a pressure of 5.7×10^{-6} bar. For each calibration a sample was taken from this large volume by connecting it with a small (1 cm^3) volume (figure 2). The known nitrogen gas content was admitted to the QMS detection system tuned to mass 14. The calibration factor gives the number of nitrogen molecules admitted to the system $P_{\rm cal}V_{\rm S}^{\rm cal}/kT$ divided by the number of counts recorded on the output side of the QMS $I_{\rm S,QMS}^{\rm cal}$: thus $f_{\rm cal} = (P_{\rm cal}V_{\rm S}^{\rm cal}/kT)/I_{\rm S,QMS}^{\rm cal}$, where $P_{\rm cal}$ is the pressure inside the calibration volume $V_{\rm S}^{\rm cal}$.

The amount of released nitrogen molecules in the desorption chamber during a desorption cycle was determined from

$$N_{\rm N2}^{D} = f_{\rm cal} I_{\rm S,QMS}^{D}, \tag{1}$$

where $I_{\rm S,QMS}^{D}$ is the time integrated intensity of the N line on the output side of the QMS (in counts). The calibration factor usually amounted to $f_{\rm cal} = 2.7 \times 10^{16}$ mol $mbar^{-1}$ cm^{-3}. The

sensitivity of the method is around 10^{13} N_2 desorbed molecules. However, the accuracy of the estimations deteriorated with increase of the temperature because the background increased as well. Knowing the amount of the outgassed nitrogen molecules, the readings of the membrane manometer, which indicates the total pressure, was calibrated with the correction for the presence of other gases.

3. Results

The HRTEM images displayed in figure 1 show the development of the grains during *in situ* heat treatment. The grain in the centre of the image grows from about 5 to 15–20 nm after treatment at 473 K for 25 min followed by 523 K for 20 min. The resulting grain, however, does not look like a homogeneous entity. The inhomogeneity could be correlated with PBA and TDS observations discussed below.

To simplify the treatment of the PBA experimental data, the shape of the peak in annihilation γ-quanta spectra is characterized by the parameters S and W [13]. The main contribution to the central area of the peak (S) is due to annihilation with low momentum valence and unbound electrons, while the wings (W) are due to annihilation with high momentum core electrons. Thus, the S value is higher for a material with a lower average atomic number Z or with a higher concentration of vacancy type defects. For the parameter W this relation is reversed. In general, positrons are trapped at sites with low electron density in a material, e.g. vacancies, vacancy clusters, open-volume sites at interfaces and at voids, if present. The annihilation characteristics depend also on the presence of gases and the nature of the atoms surrounding the trapping site [13].

In figure 4, the S and W values, corresponding to the positron annihilation in the film, are plotted as a function of the temperature of the *in situ* thermal treatment. The parameter W decreases sharply with the treatment at 473 K and continues to decrease with increasing annealing temperature. In contrast, the S value systematically increases with the heat treatment.

This observation is in contrast with a simple picture of nitrogen release: an increase in average atomic number Z in the film would lead to an increase of the W value, as was observed in γ'-Fe_4N samples after reduction in a H_2 atmosphere [14]. Similarly, the increase of the S value seems to be in disagreement with a model of growth of larger, perfect grains from small nanocrystallites and amorphous intergranular material during the heat treatment. Evidently, the tendency is opposite; during the grain growth the mismatch between the grains increases and positron trapping centres are created with lower electron density. These can be voids formed during heat-induced nitrogen release. The voids could be the cause of the inhomogeneities in the HRTEM image in figure 1, mentioned above.

In figure 5 the amount of desorbed N_2 molecules versus the substrate temperature is plotted. The enhancement of the TDS yield can be noted at four temperatures, T_1–T_4, with the maximum release rate at 800 K. The sample after this treatment was almost free from nitrogen as followed from XRD: the (011) peak had no shift with respect to the position of the (011) α-Fe line; see figure 6. This means that all the nitrogen relocated from the crystalline matrix after the heating at 800 K.

The loss of nitrogen combined with grain growth has a dramatic effect on the magnetic properties. In figure 7 the hysteresis loops are shown for the sample before and after the TDS experiment. The hysteresis loops were measured with the magnetic field applied along and perpendicular to the easy axis. The opening of the hysteresis loops, or coercive field H_c, for the as-deposited sample was about 1 Oe. The tilt of the loop for the field applied in the hard direction characterizes the uniaxial anisotropy field, $H_k \approx 30$ Oe; figure 7(a). After the TDS

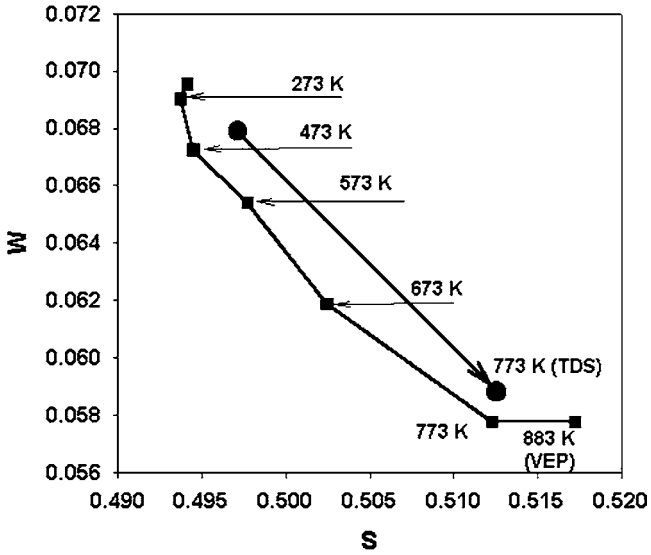

Figure 4. An *S*–*W* plot of the PBA data for a sample annealed *in situ* at the temperatures indicated for 30 min (squares). Also *S*–*W* is plotted (circles) for the sample before and after TDS.

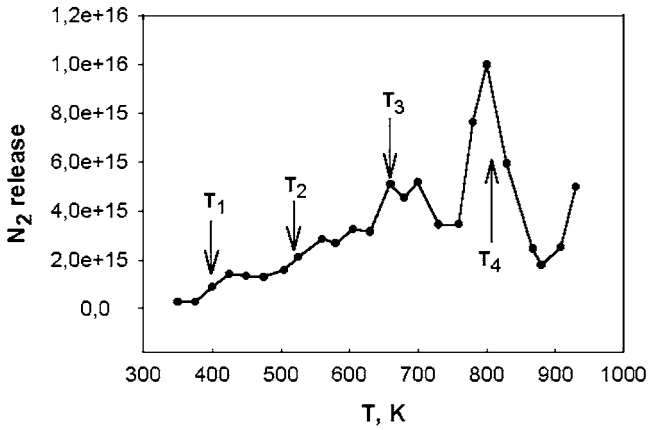

Figure 5. Amount of released molecules versus the annealing temperature.

treatment, the coercive field H_c increased to 18 Oe and the uniaxial anisotropy field completely vanished; see figure 7(b).

4. Discussion

In previous work we have shown that the presence and location of nitrogen in the matrix correlates with the grain size and that both have a drastic effect on magnetic properties [15]. The present results, figure 7, support these findings. The nitrogen release during annealing from Fe-based materials has been studied in [16–18] whereas this study differs from previous works in the initial structure and composition of the materials.

None of the publications, to the best of our knowledge, has dealt with nitrogen thermal desorption from nanocrystalline Fe-based materials. It is well established [7, 15, 19] that during

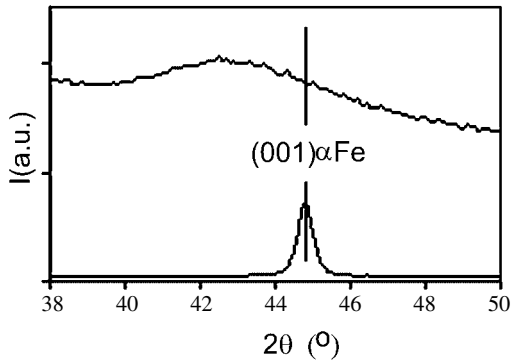

Figure 6. XRD from the sample spectra prior to and after TDS.

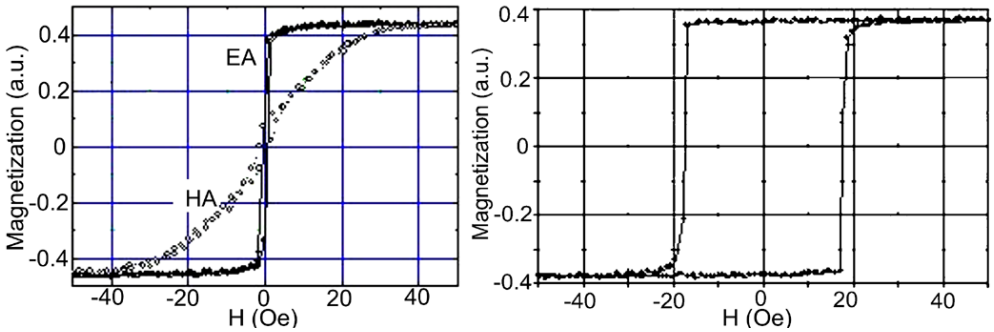

Figure 7. Hysteresis loops for the sample prior to (a) and after (b) TDS treatment.

the sputter deposition most of the nitrogen occupies interstitial positions in nanocrystalline α-Fe, even within grains a few nanometres in size, causing the shift of the (001) α-Fe line. Though the initial nitrogen content in our nanocrystalline Fe–Zr–N films was high enough to transform the whole film to γ'-phase, only faint satellites around α-Fe lines, which could be assigned to nitrides, were observed in the TEM diffraction patterns. The satellites appeared at about 500 K and disappear at 750 K. None of the second phases was distinctly observed by means of XRD.

The simplest model for the nitrogen release assumes a homogeneous film from which interstitial nitrogen migrates to the surface. If the process is diffusion limited, i.e. the recombination at the outer surface is fast, the characteristic time for the release is given by [20, 21]

$$\tau = (2d)^2/(\pi^2 D) \tag{2}$$

with $D = D_0 \exp(-E_m/kT)$ where d is the film thickness. Taking the diffusion parameters for the bulk α-Fe [22], $D_0 = 7.8 \times 10^{-3}$ cm^2 s^{-1}, $E_m = 0.82$ eV, yields for $T = 400$ K $D = 3.6 \times 10^{-13}$ cm^2 s^{-1} and $\tau = 112$ s; i.e. all the nitrogen would have been released during our experiments even at this low temperature. In fact this did not happen. Only a small fraction of nitrogen out-diffused in the temperature range $T_1 = 400$–500 K, according to figure 5, indicating that the process is still operative but suppressed. Thus, bulk diffusion as the sole mode of nitrogen migration to the surface does not work. Most of the nitrogen is bound more strongly and a larger activation energy is required than for the bulk diffusion.

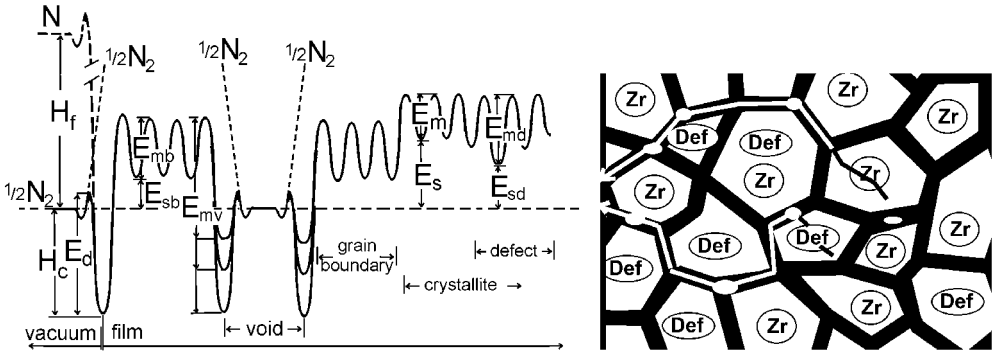

Figure 8. The energy profile for nitrogen in nanocrystalline Fe–Ze–N film is shown in the left panel. Possible trajectories of the diffused nitrogen are shown in the right panel by zigzag paths. The trapping sites are schematically indicated as ovals (for voids at the grain boundaries), 'Zr' (for Zr atoms) and 'Def' (for other types of trapping defect).

Table 1. Main activation parameters of nitrogen interaction with iron.

Notation	Activation energies	Value (eV/atom)	References
E_m	N migration in bulk α-Fe	0.82	[22]
E_s	Heat of solution	$(0.36 + 4.3) \times 10^{-4}$ T	[22]
H_c	Enthalpy of chemisorption		
E_d	Activation energy for	2.1–2.3	[23, 24]
	recombination and desorption	0.5–2.2 (depending on coverage)	[25]
H_f	Enthalpy of dissociation $N_2 \rightarrow 2N$	10.2	[26]

Evidently, the process of out-diffusion in nanocrystalline materials is more complicated: one can identify several traps, which can retard the diffusion. Interstitial nitrogen moving in the nanograin can be retrapped by the dissolved Zr. At the grain boundary it can be collected in cavities (bubbles) filled with nitrogen molecular gas and with surface chemisorbed nitrogen on the inner walls. Transport via grain boundaries will be retarded by trapping in the bubbles and cavities. Figure 8 shows schematically the energy profile, which illustrates the trapping sites for nitrogen in nanocrystalline Fe–Zr–N discussed below. The energy of the system is given for a nitrogen atom or $1/2$ nitrogen molecule when it is placed at different sites in the nanocrystalline system. The notation for the activation energies and enthalpies, used in the figure, is explained in tables 1 and 2. As in a bulk material, atomically dissolved interstitial nitrogen becomes mobile, overcoming the barrier E_m (figure 8). In the Fe–Zr–N alloy, Zr atoms provide sites with a binding energy as high as $H_{Zr-N} = 3.8$ eV/atom [22], when ZrN precipitates are formed. However, the concentration of 1–2 at.% Zr was too small to bind a significant amount of nitrogen. The binding energy for the second and further neighbouring atoms is not expected to be as high. Immobile defects could provide the trapping sites, forming nitrogen–defect complexes.

The grain boundaries, which can take up a significant volume fraction in nanocrystalline media, can also play an important role in retarding the nitrogen diffusion by formation of cavities filled with nitrogen released from the grains. It is often reported in the literature that diffusion along grain boundaries is fast (see for example [27]). However, in our case it does not prevent an agglomeration of the nitrogen on grain boundaries. In the energy profile, figure 8, it is indicated that the energies for overcoming defects and grain boundaries, E_{md} and E_{mb}, respectively, will be larger than E_m. PA results indicate that at high annealing temperatures the

Table 2. Activation energies for the main rate limiting processes in nitrogen desorption as obtained in this work.

T (K)	Assigned to	Activation energy (eV/atom)
$T_1 = 400$–425	Bulk migration	$E_{\mathrm{m}} = 0.82 \pm 0.05$
$T_2 = 525$–550	Defect binding	$E_{\mathrm{md}} = 1.23 \pm 0.05$
$T_3 = 675$–725	Grain boundary/γ'-decay	$E_{\mathrm{mb}} = 1.31 \pm 0.05$
$T_4 = 775$–825	Void release	$E_{\mathrm{mv}} = 2.3 \pm 0.05$
$T = 400$–825	Grain growth	$E_{\mathrm{gg}} = 0.5 \pm 0.1$

free volume increases and cavities could be formed. It should be noted that at certain stages the cavities are saturated with nitrogen and contain also molecular nitrogen gas as surface chemisorbed nitrogen. If recombination of atomic nitrogen into molecular nitrogen is possible in such voids, then a much larger energy E_{mv} is required for dissociation and further diffusion of nitrogen to the surface.

At a given temperature, the transport of nitrogen takes place between sites with the characteristic activation energy E_{mk}, where the subscript k stands for d (defect-limited diffusion), b (grain-boundary-limited diffusion) and v (void/cavity-limited diffusion). A fraction of nitrogen, which becomes mobile due to release from the sites with lower activation energies, will be trapped at higher binding sites. The pre-exponential factor in the diffusion coefficient is determined by the jump distance. As a rough approximation, we can assume that the jump distance, L_{k}, is determined by the average distance between the k traps, i.e. neglecting all intermediate jumps (which require much lower activation energy) between the sites with lower binding energies. One can define an effective diffusivity for trapping mediated diffusion

$$D_{\mathrm{k}}(T) \cong D_{0\mathrm{k}} \exp[-E_{\mathrm{mk}}/(RT)], \tag{3}$$

where $D_{0\mathrm{k}} \cong (1/6)L_{\mathrm{k}}^2 \nu_{\mathrm{k}}$, assuming three-dimensional diffusion with ν_{k} the attempt frequency for dissociation from trap k. For detrapping from small defects, ν_{k} is of the order of the Debye frequency (10^{13} s^{-1}), but for detrapping from bubbles, ν_{k} can be orders of magnitude smaller.

One should take into account that during the nitrogen release process and cavity formation the grain size may also increase. Roughly, the grain growth is assumed to follow the relation [27, 28]

$$L^n - L_0^n = Kt. \tag{4}$$

Here we assume $n = 2$ and that the grain growth rate coefficient, K, is determined by the corresponding activation energy E_{gg} and by the temperature, so

$$K = K_0 \exp[-E_{\mathrm{gg}}/(RT)], \tag{5}$$

where K_0 and E_{gg} have to be determined from the experimental results. From the fit to the HRTEM data, we estimate the initial grain size $L_0 = 5$ nm, $K_0 = 1 \times 10^3$ nm^2 s^{-1} and $E_{\mathrm{gg}} = 0.5 \pm 0.1$ eV/atom.

In summary, the nitrogen release occurs as follows:

(1) Up to 425 K, there are no big changes in coercive and anisotropy fields. Thus most of the nitrogen was kept interstitially, though a tiny fraction of it was released in the temperature interval $T_1 = 400$–425 K, as observed by TDS (note the log scale in figure 5), which could be ascribed to the most weakly bound nitrogen in a regular α-Fe environment. No grain growth was observed with TEM and there was no change in the parameter S and almost no change in W in the PBA.

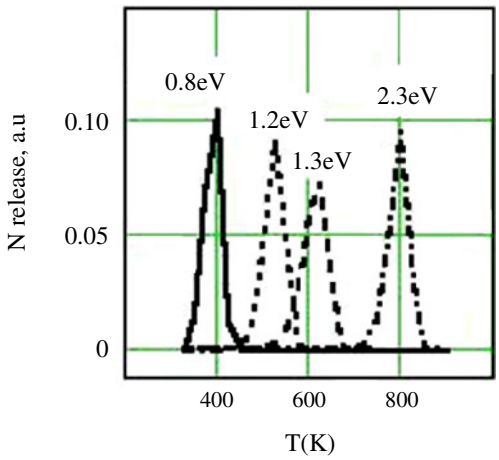

Figure 9. The temperature dependence of the released nitrogen for different activation energies ($E = q \times 0.82$ eV/atom, where $q = 1.0$, 1.5, 1.6 and 2.8).

(2) At somewhat higher temperature $T_2 = 525$–550 K, TDS reveals some minor outgassing (see figure 5) and PBA (figure 4) indicates the formation of free volume. The nitrogen release increase at T_2 could be interpreted as an activation of the nitrogen trapped by immobile defects or by Zr atoms.
(3) The desorption at $T_3 = 675$–725 K can be connected with a decay of the γ'-Fe_4N phase. This effect corresponds to the decay of satellite lines observable in SAED TEM.
(4) During all these stages and up to the region $T_4 = 775$–825 K, besides the diffusion, accumulation of nitrogen in the intergranular boundaries and formation of nanosized cavities/bubbles also occur. As illustrated in figure 8, the binding energy of an N atom at the cavity wall reduces with increase of the coverage and at certain saturation coverage of the void walls the dynamic recombination $2N \leftrightarrow N_2$ is favourable.

Taking into account the sequential temperature scheme followed during the annealing described in section 2.2, the calculated nitrogen release for different diffusion processes is plotted in figure 9. The activation energies, fitted to the gas release enhancement temperatures T_1–T_4, are given in table 2, together with attempted assignments to the related mechanisms. For the defect trapping we assume the jumping distance estimated from a defect concentration equal to that of Zr, i.e. 2 at.%. For the void trapping release the jump distance was assumed to be equal to the grain size, which follows the temperature dependence, equations (4) and (5). The attempt frequency was assumed to be the Debye frequency. From table 2 one can see that the activation energy for release at 800 K is 2.8 times higher than the migration energy E_m in the bulk single crystalline α-Fe, i.e. $E_{mv} = 2.8E_m = 2.3$ eV/atom. Such a high value of the activation energy is close to the activation energy for recombination and desorption of nitrogen on the iron surface (see [23–25] and table 1), suggesting that the absorption of nitrogen with decomposition of molecules plays an important role in the diffusion and supporting the idea of a void trapped mechanism. We note that the activation energies listed in table 2 do not critically depend on the jump distance or attempt frequency values. The corresponding uncertainties, in essence, are included in the errors indicated for the activation energies.

The thin films stay magnetically soft as long as the nitrogen stays within the crystallites. As soon as it relocates to the grain boundaries, the soft properties will deteriorate. According to the specification in table 2, this happens at temperatures higher than T_2, in agreement with the magnetic characterization data [19].

5. Conclusions

Summarizing, we have reported on the compositional and microstructural changes caused by thermal treatments in sputter-deposited nanocrystalline ultrasoft magnetic $(Fe_{98}Zr_2)_{1-x}N_x$ films. Using HRTEM with an *in situ* thermal treatment, we demonstrated grain growth. From PBA study we have learned that the free volume increases during the annealing in contrast to expectation based on a simple model of the grain growth and nitrogen released. The increase of the free volume can be connected with the relocation of the nitrogen to the periphery of the grains with formation of nanosize voids. From TDS data, we see that nitrogen starts to outgas even at slightly elevated temperatures. However, this fraction is low, indicating only a small degree of porosity of the films. This is in accordance with the excellent ultrasoft magnetic properties of our films. Most of the nitrogen escapes from the sample at temperatures around 800 K. We also note that the sample surface remains smooth after the TDS experiment, indicating that the size of the bubbles remains small, so no blistering occurs. It is possible that at temperatures higher than $T = 600\,^{\circ}\mathrm{C}$ the voids left by the escape of nitrogen start to recover. An indication of that is given by the constancy of the W value between $T = 500$ and $600\,^{\circ}\mathrm{C}$.

Acknowledgments

This work was supported by the Dutch Stichting Technische Wetenschappen (STW), the Prioriteitsprogramma Materialenonderzoek (PPM) and by the Netherlands Institute of Metal Research (NIMR). NGCh acknowledges partial support from the grant NSh-1619.2003.2 from the President of RF. Mr Kees Westerduin is acknowledged for performing TDS measurements.

References

[1] Hoffmann H 1979 *Thin Solid Films* **58** 223
Hoffmann H 1964 *J. Appl. Phys.* **35** 1790
[2] Herzer G 1995 *Scr. Metall. Mater.* **33** 1741
[3] Viala B, Minor M K and Barnard J A 1996 *J. Appl. Phys.* **80** 3941
[4] Wang H Y, Yang E Y, Bai H L, Wu P, Wang Y and Gong F F 1997 *J. Phys.: Condens. Matter* **9** 8443
[5] Jin S, Zhu W, Tiefel T H, Korenivski V, van Dover R B and Chen L H 1997 *J. Appl. Phys.* **81** 4042
[6] Shimizu O, Nakanishi K and Yoshida S 1991 *J. Appl. Phys.* **70** 6244
[7] Chezan A R, Craus C B, Chechenin N G, Niesen L and Boerma D O 2002 *Phys. Status Solidi* a **189** 833
[8] Sun N X, Crawford A M and Wang S X 2002 *MRS Symp. Proc.* **721** E6.3
[9] Crawford A M, Gardner D and Wang S X 2002 *Trans. Magn. Soc. Japan* **2** 357
[10] Chechenin N G, van Veen A, Schut H, Chezan A R, Boerma D O, Vystavel T and De Hosson J Th M 2002 *MRS Symp. Proc.* **721** 185
[11] Arnoldbik W M and Habraken F H P M 1993 *Rep. Prog. Phys.* **56** 859
Barbour J C and Boyle B L 1995 *Handbook of Modern Ion Beam Materials Analysis* (Pittsburgh, PA: Materials Research Society) chapter 5
[12] Chechenin N G, Craus C B, Chezan A, Vystavel T, Boerma D O, De Hosson J Th M and Niesen L 2002 *IEEE Trans. Magn.* **38** 3027
[13] van Veen A, Schut H and Mijnarends P E 2000 *Positron Beams and Their Applications* ed P G Coleman (Singapore: World Scientific) pp 191–225
[14] Chechenin N G, van Veen A, Escobar Galindo R, Shut H, Chezan A R, Bronsveld P M, De Hosson J Th M and Boerma D O 2001 *J. Phys.: Condens. Matter* **13** 5937
[15] Chezan A, Craus C B, Chechenin N G, Vystavel T, Boerma D, De Hosson J Th M and Niesen L 2002 *IEEE Trans. Magn.* **38** 3144
[16] van Veen A, Westerduin K T, Schut H, Melker E J E, Thijsse B J, Nielsen B, Asoka-Kumar P, Ghosh V J and Lynn K G 1997 Microstructure evolution during irradiation *MRS Symp. Proc.* **439** 407
[17] Chatbi H, Vergnat M, Bobo J F and Hennet L 1997 *Solid State Commun.* **102** 677

[18] Belmonte T, Bockel S, Bordot C, Ablitzer D and Michel H 1998 *Appl. Surf. Sci.* **135** 259
[19] Chezan A R 2002 Nanostructure and soft magnetic properties of iron–nitrogen alloys *PhD Thesis* University of Groningen
[20] Crank J 1957 *The Mathematics of Diffusion* (Oxford: Clarendon)
[21] Shewmon P G 1963 *Diffusion in Solids* (New York: McGraw-Hill)
[22] Fromm E and Gebhardt E 1976 *Gase und Kolenstoff in Metallen* (Berlin: Springer)
[23] Bozso F, Ertl G, Grunze M and Weiss M 1977 *J. Catal.* **49** 18
[24] Bozso F, Ertl G, Grunze M and Weiss M 1977 *J. Catal.* **50** 519
[25] Scholten J J F, Zwietering P, Konvalinka J A and Boer J H 1959 *Trans. Faraday Soc.* **55** 2166
[26] Weast R C and Astle M J (ed) 1983 *Handbook of Chemistry and Physics* 63rd edn (Boca Raton, FL: CRC Press) p F-195
[27] Christian J W 1975 *The Theory of Transformation of Metals and Alloys* (Oxford: Pergamon)
[28] Callister W D Jr 1997 *Materials Science and Engineering. An Introduction* (New York: Wiley)